

# Millicharged particles from proton bremsstrahlung in the atmosphere

Mingxuan Du,<sup>1</sup> Rundong Fang,<sup>1</sup> and Zuowei Liu<sup>1,2</sup>

<sup>1</sup>*Department of Physics, Nanjing University, Nanjing 210093, China*

<sup>2</sup>*CAS Center for Excellence in Particle Physics, Beijing 100049, China*

Light millicharged particles can be copiously produced from meson decays in cosmic ray collisions with the atmosphere, leading to detectable signals in large underground neutrino detectors. In this paper we study a new channel to produce millicharged particles in the atmosphere, the proton bremsstrahlung process. We find that the proton bremsstrahlung channel can produce a much larger flux of millicharged particles than the previously studied meson decay channel, resulting in an improvement on the SuperK limit by nearly one order of magnitude. Consequently, SuperK can probe new parameter space beyond the current leading limits from ArgoNeuT. We further note that the study on the proton bremsstrahlung process can be extended to other atmospherically produced light particles, and to millicharged particle searches in proton accelerators.

## I. INTRODUCTION

Although the standard model (SM) has achieved remarkable success in describing the microscopic world, there are overwhelming evidences pointing to the existence of new physics beyond the standard model (BSM). Recently, a great amount of effort has been devoted to BSM models with a dark sector (or hidden sector) that only has portal interactions with the SM sector [1]. Light dark sector particles with mass in the MeV-GeV range can still have a somewhat sizable coupling to the SM sector, despite the great progress both in the energy and intensity frontiers [2, 3]. One class of such new particles is called millicharged particles (MCPs), which interact with the SM photon via a small electric charge [4, 5].

MCPs can naturally arise in models with a “hypercharge portal”, which can be materialized either in a kinetic mixing portal [6–8], or in a Stueckelberg portal [9–11]. Recently, searches for MCPs have been pursued extensively both in astrophysics and cosmology and in accelerator experiments on Earth. For light MCPs with mass  $\lesssim$  MeV, the stringent constraints mainly come from stellar evolution [12–19] and big bang nucleosynthesis [14–18]. Constraints on MCPs with mass above MeV are dominated by accelerator experiments, including fixed target experiments with an electron beam [20–26] and with a proton beam [27–29], and collider experiments [14, 18, 30–32]. Recently, a number of new search strategies for MCPs have been proposed [33–46]. We note that dark matter (DM) can be millicharged [10, 11, 47–49], which may provide an interpretation to the recent EDGES 21 cm anomaly [50–61].

One interesting probe of MCPs, which has been studied recently [62–64], is through collisions between cosmic rays and the atmosphere [65]. The large underground neutrino detectors such as SuperK are the ideal experiments to detect atmospheric MCPs, which can lead to competitive limits [62]. However, only the MCP flux from meson decays (MD) in the atmospheric air shower has been considered in Refs. [62–64]. In this paper we consider another important channel to produce MCPs in the atmosphere: the proton bremsstrahlung (PB) pro-

cess. The MCP production diagram in the PB process is shown in Fig. (1), where a pair of MCPs are radiated from the proton, when it collides with nuclei in the atmosphere.

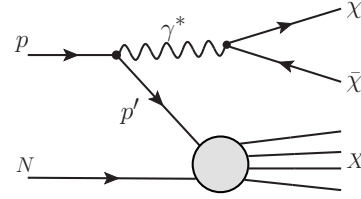


Figure 1. Feynman diagram to produce MCP  $\chi$  in the proton bremsstrahlung process in collisions between the cosmic proton  $p$  and the nucleus  $N$  in the atmosphere.

The PB process is often computed in the Fermi-Weizsäcker-Williams (FWW) approximation [66–68]; see e.g., Refs. [69–74] for recent calculations of the PB process in accelerators, which can lead to competitive contributions to dark photons as the MD process. However, the FWW approximation requires relativistic and collinear conditions for initial and final state particles, which may not be satisfied in atmospheric collisions. To take into account the contributions from low energy protons, which are the dominant component of the cosmic rays, we develop a new method to compute the PB process. We find that the dominant production channel for the atmospheric sub-GeV MCPs is the PB process, rather than the previously studied MD process. Consequently, the SuperK constraints on  $\varepsilon^2$  for sub-GeV MCPs are improved by about one order of magnitude, when the PB process is taken into account. This then provides the leading constraints for MCPs with mass  $\lesssim$  0.7 GeV, as shown in Fig. (2).

## II. ATMOSPHERIC MCP FLUX

To study atmospheric MCPs, we consider a low energy phenomenological model such that the MCP is the only new particle in the dark sector, which is usually assumed

in various terrestrial studies on MCPs. The interaction Lagrangian between the MCP  $\chi$  and the SM photon  $A_\mu$  is  $\mathcal{L}_{\text{int}} = \varepsilon e A_\mu \bar{\chi} \gamma^\mu \chi$ , where  $e$  is the QED coupling constant, and  $\varepsilon \ll 1$  is the millicharge.

To compute the MCP flux at the surface of the Earth, we use the one-dimensional approximation (see e.g., Refs. [75–77]) such that the final state particles produced in proton-air collisions are assumed to have the same direction as the incident proton. We further neglect the small attenuation effects of the atmosphere on MCPs. Cosmic protons, however, interact so strongly with the atmosphere that they are effectively absorbed before reaching the ground. This leads to an isotropic MCP flux on the Earth surface for the zenith angle  $\theta_s < \pi/2$ . Thus, in this analysis, we will only compute the MCP flux on the surface of Earth with the zenith angle  $\theta_s = 0$  (due to collisions from protons that have a vertically downward momentum, in the one-dimensional approximation), which is then taken to be the flux for all directions with  $\theta_s < \pi/2$ .

The MCP flux on the Earth surface for the zenith angle  $\theta_s = 0$  can be obtained by the cascade equation [75]

$$\frac{d^2 \Phi_\chi^s}{dE_\chi^s d\Omega_\chi^s} = \iint dh dE_p \frac{d^2 \Phi_p(h)}{dE_p d\Omega_p} n_T(h) \sigma_{pT} \sum_i \frac{dN_\chi^i}{dE_\chi^s}, \quad (1)$$

where  $h$  is the height,  $E_p$  is the proton energy,  $\Phi_\chi^s$  is the MCP flux at the surface of Earth,  $\Phi_p(h)$  is the proton flux at height  $h$ ,  $n_T(h)$  is the number density of air at height  $h$ ,  $\sigma_{pT}$  is the in-elastic proton-air cross section,  $dN_\chi^i/dE_\chi^s$  is the energy spectrum of  $\chi$  per proton-air interaction in the production channel denoted by  $i$ , which can be either the PB channel or the MD channel.<sup>1</sup> In our analysis we only consider proton-nitrogen collisions in the atmosphere, and adopt a constant  $\sigma_{pT} \simeq 253$  mb [78, 79], since the cross section has a weak dependence on the proton energy. We use the NRLMSISE-00 atmosphere model [80] for the air density  $n_T(h)$ . The cosmic ray proton flux at the top of the atmosphere can be well approximated by a power law [81]:

$$\frac{d^2 \Phi_p}{dE_p d\Omega_p}(h_{\text{max}}) = \frac{0.74 \times 1.8 \times 10^4}{\text{m}^2 \text{ s sr GeV}} \left( \frac{E_p}{\text{GeV}} \right)^{-2.7}, \quad (2)$$

where  $h_{\text{max}} = 65$  km.<sup>2</sup> We obtain the proton flux at height  $h$  by using the cascade equation [75]

$$\frac{d}{dh} \left[ \frac{d^2 \Phi_p}{dE_p d\Omega_p}(h) \right] = \sigma_{pT} n_T(h) \frac{d^2 \Phi_p}{dE_p d\Omega_p}(h). \quad (3)$$

<sup>1</sup> We provide our MD calculation, and the comparison with Refs. [62–64] in Appendix A.

<sup>2</sup> We have also carried out analyses by using the cosmic ray data [81], which agrees with the power-law spectrum; see Appendix B for the comparison.

### III. MCPS IN THE PB CHANNEL

The energy spectrum of MCPs in the PB process can be computed by [24]

$$\frac{dN_\chi^{\text{PB}}}{dE_\chi} = \frac{\varepsilon^2 e^2}{6\pi^2} \int \frac{dk^2}{k^2} \sqrt{1 - \frac{4m_\chi^2}{k^2}} \left( 1 + \frac{2m_\chi^2}{k^2} \right) \times \int dE_k \frac{1}{\sigma_{pT}} \frac{d\sigma_{\text{PB}}}{dE_k} \frac{\Theta(E_\chi - E_-) \Theta(E_+ - E_\chi)}{E_+ - E_-}, \quad (4)$$

where  $m_\chi$  is the mass of the MCP. Here  $d\sigma_{\text{PB}}/dE_k$  is the cross section of the  $pN \rightarrow \gamma^* X$  process with the following sum rule for the off-shell photon  $\gamma^*$  [82]

$$\sum_i \epsilon_\mu^i(k) \epsilon_\nu^{i*}(k) = -g_{\mu\nu} + \frac{k_\mu k_\nu}{k^2}, \quad (5)$$

where  $k^\mu = (E_k, \vec{k})$  is the photon momentum, and  $X$  denotes the final state particles besides the off-shell photon  $\gamma^*$ . The maximal and minimum energies of MCPs are given by  $E_\pm \equiv \gamma(E_\chi^r \pm \beta p_\chi^r)$  where  $\gamma = (1 - \beta^2)^{-1/2} = E_{\gamma^*}/\sqrt{k^2}$ , and  $E_\chi^r$  ( $p_\chi^r$ ) is the energy (magnitude of momentum) of MCPs in the rest frame of the off-shell virtual photon.

The cross section  $d\sigma_{\text{PB}}/dE_k$  in the PB process  $pN \rightarrow \gamma^* X$  is often computed in the FWW approximation [66–68], in which relativistic and collinear conditions are assumed for the protons and the photon [69–74, 83, 84]. These conditions are excellent approximations to physics in accelerators with an energetic proton beam. However, for the cosmic rays, the low energy protons are the dominant component of the cosmic flux, as indicated by the power law of  $E^{-2.7}$ . In an attempt to take into account the low energy protons, we develop a new method to compute the PB process. We compare our method with the FWW approximation in the Appendix B.

In our method, we first compute the splitting kernel for the  $p \rightarrow \gamma^* p$  process, by taking the ratio of the differential cross section of the 2-to-3 process,  $p(p_1)\bar{p}(p_2) \rightarrow p(p_3)\bar{p}(p_4)\gamma^*(k)$ , where the momentum for each particle is given inside the parenthesis, to the total cross section of the corresponding 2-to-2 process,  $p\bar{p} \rightarrow p\bar{p}$ . Both processes are mediated by an s-channel photon. Thus one has<sup>3</sup>

$$\frac{d^2 \mathcal{P}_{p \rightarrow \gamma^* p}}{dE_k \cos \theta_k} = \frac{1}{\sigma(p\bar{p} \rightarrow p\bar{p})} \frac{d^2 \sigma(p\bar{p} \rightarrow \gamma^* p\bar{p})}{dE_k \cos \theta_k}, \quad (6)$$

where  $\sigma(p\bar{p} \rightarrow p\bar{p})$  is evaluated at  $s_{34} = (p_3 + p_4)^2$ . We first evaluate the splitting kernel in the CM frame,

$$\frac{d^2 \mathcal{P}_{p \rightarrow \gamma^* p}}{dE_k^0 d \cos \theta_k^0} = \frac{|F_V(k)|^2}{\sigma_{2 \rightarrow 2}(s_{34})} \frac{\int dE_3^0 \int d\phi_{3,k}^0 |\overline{\mathcal{M}}_{2 \rightarrow 3}|^2}{512\pi^4 E_1^0 E_2^0 |\vec{v}_1^0 - \vec{v}_2^0|}, \quad (7)$$

<sup>3</sup> See also Ref. [73] for a similar treatment, but for t-channel pomeron exchange diagrams in relativistic limits.

where  $F_V$  is the vector meson form factor,  $\mathcal{M}_{2\rightarrow 3}$  is the matrix element of the  $p\bar{p} \rightarrow \gamma^* p\bar{p}$  process,  $\sigma_{2\rightarrow 2}(s_{34})$  is the cross section of the  $p\bar{p} \rightarrow p\bar{p}$  process,  $E_3^0$  is the energy of the final state proton,  $\phi_{3,k}^0$  is the azimuth angle of  $\vec{p}_3$  in the transverse plane of  $\vec{k}$ , and  $\theta_k^0$  is the angle between  $\gamma^*$  and the initial state proton. We only consider the initial radiation diagrams in computing the  $\mathcal{M}_{2\rightarrow 3}$  matrix element so that the splitting kernel is compatible with the process shown in Fig. (1). We then use the resulting splitting kernel to compute the differential cross-section  $d\sigma_{\text{PB}}/dE_k$  of the  $pN \rightarrow \gamma^* X$  process in the lab frame:

$$\frac{d\sigma_{\text{PB}}}{dE_k} = \int dE_k^0 d\cos\theta_k^0 \frac{d^2\mathcal{P}_{p\rightarrow\gamma^*p}}{dE_k^0 d\cos\theta_k^0} \sigma_{pT}(s'_2) \delta(E'_k - E_k), \quad (8)$$

where  $\sigma_{pT}$  is the proton-nitrogen cross section evaluated at  $s'_2 = (p_p + p_N - k)^2$  with  $p_p$  ( $p_N$ ,  $k$ ) being the momentum of the proton (nitrogen, photon). Here  $E'_k = \gamma(E_k^0 - \beta|\vec{p}_k^0|\cos\theta_k^0)$  where  $\gamma = 1/\sqrt{1-\beta^2}$ , and  $\beta$  is the relative velocity between the lab frame and the CM frame.

In the above calculation, we have included for the  $p\gamma^*p$  vertex the time-like form factor due to several light vector mesons [70, 72–74, 85]

$$F_V(k) = \sum_{V=\rho\rho'\rho''\omega\omega'\omega''} \frac{f_V m_V^2}{m_V^2 - k^2 - im_V \Gamma_V}, \quad (9)$$

where  $m_V$  ( $\Gamma_V$ ) is the mass (decay width) of the vector meson,  $f_\rho = 0.616$ ,  $f_{\rho'} = 0.223$ ,  $f_{\rho''} = -0.339$ ,  $f_\omega = 1.011$ ,  $f_{\omega'} = -0.881$ , and  $f_{\omega''} = 0.369$ . Because the time-like form factor is in the kinematic region  $0 < q^2 < 4m_p^2$ , which has not been probed directly in experiments with proton beams, the expressions in Eq. (9) are obtained from a vector meson dominance (VMD) model by assuming both protons in the vertex to be on-shell. Because the effects due to the off-shell-ness of the intermediate proton in the VMD model have been found to be only a few percent [86], we do not include an additional form factor for the off-shell proton as done in Ref. [73].

#### IV. EARTH ATTENUATION

To compute the MCP flux at underground neutrino detectors, one has to take into account the Earth attenuation effects. The energy loss of MCPs along a trajectory in Earth can be described by [64, 87]

$$-\frac{dE}{dX} = \varepsilon^2(a + bE), \quad (10)$$

where  $X$  is the slant depth traversed, and  $a$  ( $b$ ) is the parameter to describe energy loss due to ionization (radiation in scatterings with nuclei). We adopt the parameters for muons in the standard rock:  $a = 0.233$  GeV/mwe and

$b = 4.64 \times 10^{-4}$  mwe $^{-1}$  with 1 mwe = 100 g/cm $^2$  [88]. The slant depth traversed by MCPs can be computed by

$$X = \rho\sqrt{(R_e - d)^2 + R_e^2 - 2(R_e - d)R_e \cos(\theta - \theta_s)},$$

where  $\rho = 2.6$  g/cm $^3$  is the density of the standard rock,  $d$  is the depth of the detector,  $R_e$  is the radius of Earth,  $\theta$  ( $\theta_s$ ) is the zenith angle of the MCP viewed by the detector (the intersection point on the Earth surface) such that  $\sin\theta_s/(R_e - d) = \sin\theta/R_e$  with  $\theta_s < \pi/2$ . The MCP flux with energy  $E_\chi$  at slant depth  $X$  underground is related to the flux at the surface via [87]

$$\frac{d^2\Phi_\chi^D(X)}{dE_\chi d\Omega} = e^{\varepsilon^2 b X} \frac{d^2\Phi_\chi^s}{dE_\chi^s d\Omega^s}, \quad (11)$$

where  $E_\chi^s = (E_\chi + a/b) \exp(\varepsilon^2 b X) - a/b$ .

#### V. SIGNALS AT SUPERK

Large underground neutrino detectors are ideal places to detect light atmospheric MCPs [62–64]. In our analysis, we consider the SuperK experiment, which is a large water-Cherenkov detector with a fiducial volume of 22.5 kton of water, shielded by a 1000 m rock [89]. The dominant process to detect MCPs at SuperK is the elastic MCP-electron scattering [64]

$$\frac{d\sigma}{dE_r} = \varepsilon^2 \alpha^2 \pi \frac{E_r + 2E_\chi^2/E_r - 2E_\chi - m_e - m_\chi^2/m_e}{E_r m_e (E_\chi^2 - m_\chi^2)},$$

where  $E_\chi$  is the energy of the incident MCP,  $E_r$  is the recoil energy of the scattered electron, and  $m_e$  is the electron mass. The signal events can be obtained by

$$S_i = 2\pi n_e \mathcal{E} \int dE_r f(E_r) \int dE_\chi \int dz \frac{d^2\Phi_\chi^D}{dE_\chi dz} \frac{d\sigma}{dE_r}, \quad (12)$$

where  $z = \cos\theta$ ,  $\mathcal{E}$  is the exposure,  $2\pi$  is due to the integration over the angle  $\phi$ ,  $n_e$  is the number of electrons per unit mass of water, and  $f(E_r)$  is the detector efficiency. We use the data with the total exposure of 176 kton-year, accumulated during the three SuperK runs, with running time 1497 days, 794 days, and 562 days respectively [90]. We use the efficiency curve given in Fig. 10 of Ref. [90]. We bin the signal events using the same bins in the SuperK data: 18 bins with a 4 MeV bin width for each in the recoil energy of 16–88 MeV.

Because of the unknown background in the SuperK data, we follow Ref. [64] to take a background-agnostic approach such that only the bins in which the data events are less than MCP signal events are used to build the likelihood function. We use the Poisson distribution to compute the likelihood for each data bin

$$\mathcal{L}_i = \frac{S_i^{D_i} \exp(-S_i)}{D_i!}, \quad (13)$$

where  $D_i$  and  $S_i$  are the data events and the expected signal events in the  $i$ -th bin. The total likelihood is  $\mathcal{L} = \prod_i \mathcal{L}_i$ , and the test statistics is

$$\mathcal{TS} = -2 \log \left[ \frac{\mathcal{L}(m_\chi, \varepsilon)}{\mathcal{L}(m_\chi, \varepsilon = 0)} \right]. \quad (14)$$

We use  $\mathcal{TS} < 4.6$  to compute the 90% confidence level limit.

## VI. RESULTS

Fig. (2) shows the 90% CL limits on MCPs from SuperK, both for the MD-only process,<sup>4</sup> and for the combined contributions from the MD and PB processes. After taking into account the contributions from the PB process, the SuperK limit on  $\varepsilon^2$  is improved by an order of magnitude for the MCP mass larger than 0.1 GeV. The SuperK limit (with both MD and PB contributions) is shown to be better than the current world-leading limits from the ArgoNeuT [29], in the mass range of 0.1 – 0.7 GeV. This improvement in the SuperK limit is due to that the number of MCP signals in the SuperK from the PB process is about  $10 \sim 100$  times larger than that from the MD process. Thus the PB process is the dominant MCP production process for the sub-GeV MCP. We note a competitive limit from past experiments in this mass range [91], albeit potential systematic uncertainties. Recently, the SLAC mQ limit has been re-analyzed with the attenuation effects taken into account, which opens up some previously excluded parameter space below  $m_\chi < 0.1$  GeV [92]. For that reason, SuperK also provides the best limit on MCPs with mass 55-100 MeV,  $\varepsilon^2 < 2 \times 10^{-6}$ , surpassing MiniBooNE [27].

We note that the sudden change in the upper bound on  $\varepsilon^2$  near  $m_\chi = m_\rho/2 \sim 0.38$  GeV is primarily due to the fact that the production rate of light MCPs in the atmosphere is significantly enhanced by the electromagnetic time-like form factor  $F_V(k)$  of the  $\rho/\omega$  vector meson; for MCP with mass exceeding  $m_\rho/2$ , the invariant mass of the off-shell photon,  $\sqrt{k^2}$ , is always larger than the mass of the  $\rho/\omega$  meson so that the resonant production via the time-like form factor starts to diminish. We also note that perhaps there is a double counting between the enhancement via the  $\rho/\omega$  form factor and the production of MCPs via  $\rho/\omega \rightarrow \gamma^* \rightarrow \chi\bar{\chi}$  in the MD process [93]. However, since the PB process is much larger than the MD process for light MCPs in the MeV-GeV mass range, one should just consider the PB process and neglect the vector MD process to avoid the possible double-counting. We note that the PB process may also lead to improved limits for MCP searches in experiments with a proton beam, where only the MD process was analyzed previously.

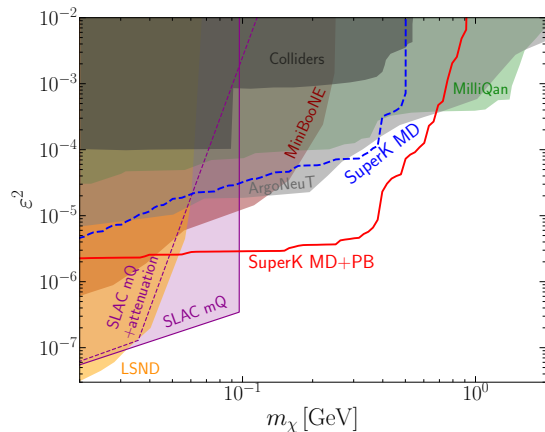


Figure 2. Super-K constraints on MCP at the 90% CL from the MD process (blue dashed curve), and from both the PB and MD processes (red solid curve). Existing constraints are shown as shaded regions: ArgoNeuT [29] (gray), MilliQan [32] (green), Colliders [18] (black), LSND [27] (orange), MiniBooNE [27] (dark red), SLAC mQ [20] (purple-solid), and the revised SLAC mQ (with attenuation effects) [92] (purple-dashed).

## VII. CONCLUSIONS

In this paper we study the PB process for the atmospheric MCP flux, which has not been considered in previous analyses, where only the MD process are included. To take into account the low energy cosmic protons, we develop a new method to compute the PB process, instead of using the FWW approximation, where protons and the emitted photon are assumed to be relativistic. We find that the PB process is the dominant production channel for sub-GeV MCPs, which can give rise to a much larger MCP flux than the previously studied MD channel. The experimental limits from SuperK are improved by a factor of (3–10) for  $\varepsilon^2$ , when the PB process is taken into account. This leads to a new leading constraint on MCPs with mass  $\lesssim 0.7$  GeV. For mass  $\lesssim 0.38$  GeV, the SuperK limit on  $\varepsilon^2$  is almost one order of magnitude better than the current best limit from the ArgoNeuT experiment. We note that the analysis presented here for the PB process can be extended to atmospheric productions of other light new particles in the hidden sector, and to MCP searches in terrestrial experiments with a proton beam.

## ACKNOWLEDGMENTS

We thank Ligang Xia and Lan Yang for discussions. The work is supported in part by the National Natural Science Foundation of China under Grant Nos. 12275128 and 12147103.

<sup>4</sup> Our MD-only limits are consistent with Refs. [62, 63], but not with Ref. [64]. See Appendix A for the detailed comparison.

## Appendix A: MCP signals from meson decays

In this appendix, we provide a brief description of our calculation of MCPs produced in the MD process, and compare it to that in Refs. [62–64]. We find that our SuperK limits (when only the MD process is considered) is in ballpark agreement with Refs. [62, 63], but is about one order of magnitude weaker on  $\varepsilon^2$  than Ref. [64]. We summarize the main differences between our calculation and Ref. [64] at the end of this section.

The calculation for the MD process is the same as the PB process, except the energy spectrum of atmospheric MCPs in Eq. (1). For the MD process, one has

$$\frac{dN_\chi^{\text{MD}}}{dE_\chi^s} = 2 \sum_m \int_1^\infty d\gamma_m \frac{dN_m(E_p)}{d\gamma_m} F_m(E_\chi^s, \gamma_m), \quad (\text{A1})$$

where  $m$  denotes the parent meson in the decay process,  $\gamma_m = E_m/m_m$  is the meson boost factor,  $dN_m(E_p)/d\gamma_m$  is the spectra of the averaged multiplicity of mesons, the factor 2 comes from the fact that two MCPs are produced in each meson decay, and  $F_m(E_\chi^s, \gamma_m)$  is the MCP energy spectra in the lab frame, which is obtained by boosting the spectra in the rest frame of meson  $m$  to the lab frame. We use the EPOS model [78] in the CRMC package [79] to compute  $dN_m(E_p)/d\gamma_m$ .

There are two types of meson decays in the atmosphere in which MCPs can be produced: pseudo-scalar meson decays, and vector meson decays, as shown in Fig. (3). In our analysis, we consider both pseudo-scalar mesons ( $\pi^0$  and  $\eta$ ) and vector mesons ( $\rho$ ,  $\omega$  and  $\phi$ ). We assume that all the mesons decay promptly, since they have very short decay length compared to the distance they travel to reach the Earth surface. For example,  $\pi^0$  has the longest lifetime  $\tau_{\pi^0} = 8.52 \times 10^{-17}$  s among the mesons we consider; the decay length of a GeV  $\pi^0$  is only  $0.2 \mu\text{m}$ .

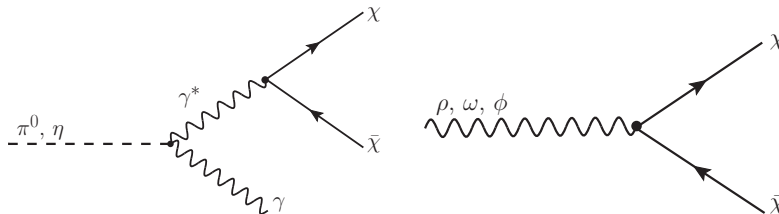


Figure 3. Feynman diagrams for MCPs productions from meson decays in the atmosphere: pseudo-scalar meson decays (left), vector meson decays (right).

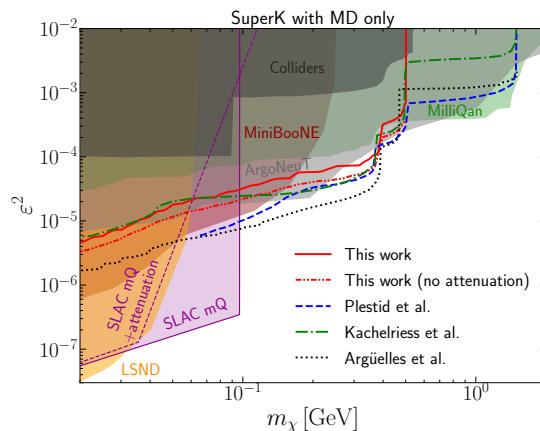


Figure 4. Super-K 90% CL constraints on MCPs with the DM channel only: our calculation (red solid curve), our calculation without the Earth attenuation (red dashdotted curve), Plestid et al. [62] (blue dashed curve), Kachelriess et al. [63] (green dashdotted curve), and Argüelles et al. [64] (black dotted curve). Existing constraints are also shown here as shaded regions: ArgoNeuT [29] (gray), MilliQan [32] (green), Colliders [18] (black), LSND [27] (orange), MiniBooNE [27] (dark red), SLAC mQ [20] (purple-solid), and the revised SLAC mQ (with attenuation effects) [92] (purple-dashed).



For the pseudo-scalar meson decay  $m \rightarrow \chi\bar{\chi}\gamma$ , one has

$$F_m(E_\chi, \gamma_m) = \int dx dy \frac{d^2 \text{Br}(m \rightarrow \chi\bar{\chi}\gamma)}{dx dy} \frac{\Theta(E_\chi - E_-) \Theta(E_+ - E_\chi)}{E_+ - E_-}, \quad (\text{A2})$$

where  $x = m_{\chi\bar{\chi}}^2/m_m^2$  with  $m_{\chi\bar{\chi}}$  being the invariant mass of the final state  $\chi\bar{\chi}$  pair,  $y = (E_\chi^r - E_{\bar{\chi}}^r)/E_\gamma^r$  with  $E_f^r$  the energy of the final state particle  $f$  in the rest frame of the meson,  $E_\pm = \gamma_m(E_\chi^r \pm \beta_m p_\chi^r)$  with  $p_\chi^r$  being the MCP momentum in the rest frame of the meson, and  $\text{Br}(m \rightarrow \chi\bar{\chi}\gamma)$  is the branching ratio. We use the Dalitz decay approach to compute the differential branching ratio [94]

$$\frac{d^2 \text{Br}(m \rightarrow \chi\bar{\chi}\gamma)}{dx dy} = \frac{\varepsilon^2 \alpha}{\pi} \text{Br}(m \rightarrow \gamma\gamma) \mathcal{F}^2(m_{\chi\bar{\chi}}^2) \frac{(1-x)^3}{4x} \left(1 + y^2 + \frac{4m_\chi^2}{m_m^2 x}\right), \quad (\text{A3})$$

where  $\alpha$  is the fine structure constant,  $\text{Br}(\pi^0 \rightarrow \gamma\gamma) \simeq 0.99$ ,  $\text{Br}(\eta \rightarrow \gamma\gamma) \simeq 0.39$  [95], and  $\mathcal{F}(m_{\chi\bar{\chi}}^2)$  is the meson form factor, which is given by [96, 97]

$$\mathcal{F}(m_{\chi\bar{\chi}}^2) = \begin{cases} 1 + a_\pi \frac{m_{\chi\bar{\chi}}^2}{m_\pi^2} & \text{for } \pi^0 \\ \frac{1}{1 - m_{\chi\bar{\chi}}^2/\Lambda_\eta^2} & \text{for } \eta \end{cases}, \quad (\text{A4})$$

where  $a_\pi = 0.0335$  [81] and  $\Lambda_\eta = 0.7191$  GeV [98].

For the vector meson decay  $m \rightarrow \chi\bar{\chi}$ , one has

$$F_m(E_\chi, \gamma_m) = \frac{\text{Br}(m \rightarrow \chi\bar{\chi})}{E_+ - E_-} \Theta(E_\chi - E_-) \Theta(E_+ - E_\chi), \quad (\text{A5})$$

where  $E_\pm = \gamma_m \left(E_m/2 \pm \beta_m \sqrt{E_m^2/4 - m_\chi^2}\right)$ . The di-MCP branching ratio is computed by rescaling the dilepton branching ratio [97]

$$\text{Br}(m \rightarrow \chi\bar{\chi}) = \varepsilon^2 \text{Br}(m \rightarrow \ell\bar{\ell}) \sqrt{\frac{1 - 4m_\chi^2/m_m^2}{1 - 4m_\ell^2/m_m^2} \frac{1 + 2m_\chi^2/m_m^2}{1 + 2m_\ell^2/m_m^2}}, \quad (\text{A6})$$

where  $\text{Br}(m \rightarrow e^- e^+) = 4.72 \times 10^{-5}$ ,  $7.36 \times 10^{-5}$  and  $2.973 \times 10^{-4}$  for  $\rho$ ,  $\omega$ , and  $\phi$  [95].

In Fig. (4), we make a comparison between our calculations in the MD channel and the results given in Refs. [62–64]. We find that our calculations yield the weakest limits (with only the MD process included). However, the attenuation effects are not discussed in Refs. [62, 63]. Our results without the attenuation effects, seem to be consistent with Refs. [62, 63]. Our limits are much weaker than Ref. [64]: For MCP mass below 0.4 GeV, the SuperK limit on  $\varepsilon^2$  obtained in our analysis (with only the MD channel is included) is higher than Ref. [64] by a factor of  $\sim 3$ . Below we summarize the main differences between our analysis in the MD channel and the analysis in Ref. [64].

1. The branching ratios into MCPs from meson decays in Ref. [64] is a factor of 2 larger than our calculations: Eq. (A3) and Eq. (A6).
2. In our calculations, we use the one-dimensional approximation, which leads to an isotropic MCP flux at the surface of Earth for  $\theta_s < \pi/2$ . Ref. [64] used a different method in which the MCP flux is found to be not isotropic at the surface of Earth.
3. We noticed an error in computing the number of electrons  $n_e$  in SuperK in [99]. The ratio between the number of electrons and the number of hydrogen in water was taken to be 18 in [99]. In our analysis, we use 10.
4. The method to compute the Earth attenuation in our analysis is different from Ref. [64].

We note that our main conclusion that the PB process is much better than the MD process for sub-GeV MCPs, should not change if one uses different methods for the attenuation and for SuperK signal events, since we have computed the PB and the MD processes with the same methods for the Earth attenuation and for the signal events in the SuperK detector.

## Appendix B: Our new PB method versus FWW

In this section, we compare the atmospheric MCP flux obtained in two different methods to compute the PB process: (1) our new method (denoted as “New PB”), and (2) the FWW approximation [66–68] (denoted as “FWW”). We also compare the SuperK constraints obtained with two different cosmic ray spectra: (1) the power law spectrum in Eq. (2) (denoted as “PL”), and (2) the actual cosmic ray data as given in PDG [81] (denoted as “PDG”).

The splitting kernel in the FWW approximation is given by [69, 83, 84]

$$\frac{d^2\mathcal{P}_{p\rightarrow\gamma^*p}^{\text{FWW}}}{dE_k d\cos\theta_k} = |\mathbf{J}(z, p_T^2)| \frac{d^2\mathcal{P}_{p\rightarrow\gamma^*p}^{\text{FWW}}}{dz dp_T^2} = |\mathbf{J}(z, p_T^2)| |F_V(k)|^2 \omega(z, p_T^2), \quad (\text{B1})$$

where  $k^\mu = (E_k, \vec{k})$  is the 4-momentum of the virtual photon,  $\theta_k$  is the angle between the virtual photon and the initial proton,  $p_T = |\vec{k}| \sin\theta_k$  is the transverse momentum,  $z = \cos\theta_k |\vec{k}| / |\vec{p}_p|$  with  $\vec{p}_p$  being the momentum of the initial proton,  $|\mathbf{J}(z, p_T^2)|$  is the determinant of the Jacobian matrix between  $(z, p_T^2)$  and  $(E_k, \cos\theta_k)$ , and  $\omega(z, p_T^2)$  is given by [69, 83, 84]

$$\omega(z, p_T^2) \simeq \frac{\alpha}{2\pi H} \left\{ \frac{1 + (1-z)^2}{z} - 2z(1-z) \left( \frac{2m_p^2 + k^2}{H} - z^2 \frac{2m_p^4}{H^2} \right) + 2z(1-z) (z + (1-z)^2) \frac{m_p^2 k^2}{H^2} + 2z(1-z)^2 \frac{k^4}{H^2} \right\}, \quad (\text{B2})$$

where  $H = p_T^2 + (1-z)k^2 + z^2 m_p^2$ . We note that the FWW approximation is valid in the relativistic and collinear limit:  $E_p, E_k, E_{p'} \gg m_p, \sqrt{k^2}, p_T$  [69–74, 83, 84]. Thus, in our analysis, we impose in the lab frame the following three conditions for the FWW approximation (denoted as the “FWW cuts”):

1.  $p_T < 0.1 E_k$  [69, 70],
2.  $p_T < 1 \text{ GeV}$  [69, 70],
3.  $|q_{\text{min}}^2| < \Lambda_{\text{QCD}}^2$  [72], where  $|q_{\text{min}}^2| \approx [p_T^2 + (1-z)k^2 + z^2 m_p^2]^2 / [4E_p^2 z^2 (1-z)^2]$  [83, 84] and  $\Lambda_{\text{QCD}} \simeq 0.25 \text{ GeV}$  is the QCD scale.

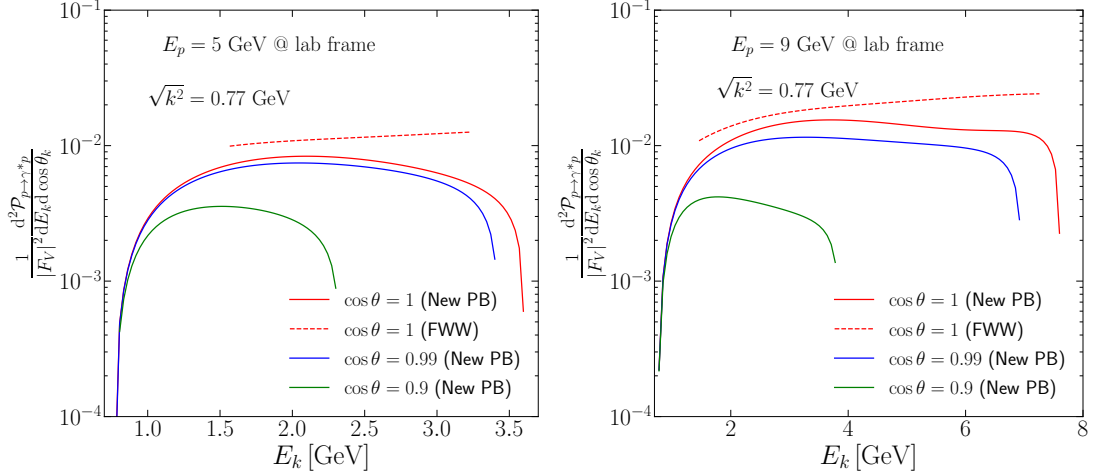


Figure 5. The splitting kernel (without the proton form factor) in the lab frame computed in our method and in the FWW approximation, for proton energy  $E_p = 5 \text{ GeV}$  (left), and for  $E_p = 9 \text{ GeV}$  (right). Three different angles in our method are plotted:  $\cos\theta = 1$  (red-solid),  $\cos\theta = 0.99$  (blue-solid), and  $\cos\theta = 0.9$  (green-solid). In the FWW approximation, we impose the “FWW cuts” (see main text), under which the splitting kernel is zero for both  $\cos\theta = 0.99$  and  $\cos\theta = 0.9$ , and thus only  $\cos\theta = 1$  (red-dashed) is shown.

In Fig. (5), we compare the splitting kernel computed in our new method with that in the FWW approximation. We consider two proton energies in Fig. (5):  $E_p = 5 \text{ GeV}$  and  $9 \text{ GeV}$ , as the low energy cosmic proton has a larger

flux. The splitting kernels in the FWW approximation is larger than our case, in the forward direction,  $\cos \theta_k = 1$ . However, the splitting kernels in the FWW approximation vanish for  $\cos \theta_k = 0.99$  and  $0.9$ , after imposing the “FWW cuts”. We also note that the low- and high-energy region of the FWW curves with  $\cos \theta_k = 1$  are not shown, which is also due to the failing of the “FWW cuts” there. Thus it is difficult to satisfy the conditions for the FWW approximation in the collisions between low energy cosmic protons and the atmosphere. Although the splitting kernel in the forward direction in the FWW approximation seems to be overestimated as compared to our method, the SuperK limits computed in the FWW approximation is weaker than our method, as shown in Fig. (6).

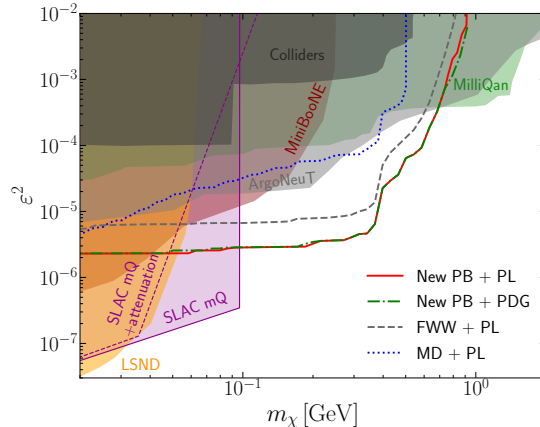


Figure 6. SuperK 90% CL limits on MCPs with the PB process: (1) our new PB method with the power law cosmic ray model in Eq. (2) (red solid curve), (2) the FWW approximation with the power law cosmic ray model (gray dashed curve), and (3) our new PB method with the cosmic ray data in Ref. [81] (green dash-dotted curve). The MD process with the power law cosmic ray model (blue dotted curve) is also shown. Existing constraints are also shown here as shaded regions: ArgoNeuT [29] (gray), MilliQan [32] (green), Colliders [18] (black), LSND [27] (orange), MiniBooNE [27] (dark red), SLAC mQ [20] (purple-solid), and the revised SLAC mQ (with attenuation effects) [92] (purple-dashed).

In Fig. (6), we compare the SuperK constraints obtained in our new method and in the FWW approximation. To speed up the calculation in the FWW approximation, we take the average energy  $E_\chi = E_k/2$  for MCPs. The SuperK upper bound on  $\epsilon^2$  computed in our method is a factor of  $\sim 2$  better than that in the FWW method (with the “FWW cuts” taken into account), for the MCP of  $0.02 \text{ GeV} \lesssim m_\chi \lesssim 0.35 \text{ GeV}$ , where the power law spectrum is used for the cosmic protons. We note that the weaker limit in the FWW method is due to the fact that a large portion of the phase space is eliminated by the “FWW cuts”, especially for low energy protons. We further note that the SuperK limits from the PB channel are significantly better than the MD channel, both in the FWW method and in our new method.

The SuperK limits from the two different profiles of cosmic protons, “PL” and “PDG”, are almost identical, where our new PB method is used, as shown in Fig. (6). Thus we mainly use the PL profile in our analysis. We note that although the amount of the cosmic protons in the PL profile at very low energy can be a factor of few larger than the actual cosmic ray data, these very low energy protons seem not to be the leading contributions to the PB process, as the limits from the two profiles are in excellent agreement with each other. This might be due to the fact that protons with energy  $\lesssim 2.6 \text{ GeV}$  (in the lab frame) are unable to radiate an off-shell photon with  $k^2$  near the  $\rho/\omega$  mass, so that the final state MCPs are not resonantly produced via the time-like form factor of the  $\rho/\omega$  vector mesons. We note that this is also in agreement with the sudden change in the limit near  $m_\chi = m_\rho/2$ .

- 
- [1] J. Alexander *et al.* 2016. [arXiv:1608.08632](#).  
[2] G. Lanfranchi, M. Pospelov, and P. Schuster, “The Search for Feebly Interacting Particles,” *Ann. Rev. Nucl. Part. Sci.* **71** (2021) 279–313 [[arXiv:2011.02157](#)].  
[3] P. Agrawal *et al.*, “Feebly-interacting particles: FIPs 2020 workshop report,” *Eur. Phys. J. C* **81** (2021) 1015

- [[arXiv:2102.12143](#)].  
[4] J. Jaeckel and A. Ringwald, “The Low-Energy Frontier of Particle Physics,” *Ann. Rev. Nucl. Part. Sci.* **60** (2010) 405–437 [[arXiv:1002.0329](#)].  
[5] M. Fabbrichesi, E. Gabrielli, and G. Lanfranchi, “The Dark Photon.” [arXiv:2005.01515](#).  
[6] B. Holdom, “Two U(1)’s and Epsilon Charge Shifts,”



- Phys. Lett. B **166** (1986) 196–198.
- [7] B. Holdom, “Searching for  $\epsilon$  Charges and a New  $U(1)$ ,” *Phys. Lett. B* **178** (1986) 65–70.
- [8] R. Foot and X.-G. He, “Comment on Z Z-prime mixing in extended gauge theories,” *Phys. Lett. B* **267** (1991) 509–512.
- [9] B. Kors and P. Nath, “A Stueckelberg extension of the standard model,” *Phys. Lett. B* **586** (2004) 366–372 [[hep-ph/0402047](#)].
- [10] K. Cheung and T.-C. Yuan, “Hidden fermion as milli-charged dark matter in Stueckelberg Z- prime model,” *JHEP* **03** (2007) 120 [[hep-ph/0701107](#)].
- [11] D. Feldman, Z. Liu, and P. Nath, “The Stueckelberg Z-prime Extension with Kinetic Mixing and Milli-Charged Dark Matter From the Hidden Sector,” *Phys. Rev. D* **75** (2007) 115001 [[hep-ph/0702123](#)].
- [12] M. I. Dobroliubov and A. Y. Ignatiev, “MILLICHARGED PARTICLES,” *Phys. Rev. Lett.* **65** (1990) 679–682.
- [13] R. N. Mohapatra and I. Z. Rothstein, “ASTROPHYSICAL CONSTRAINTS ON MINICHARGED PARTICLES,” *Phys. Lett. B* **247** (1990) 593–600.
- [14] S. Davidson, B. Campbell, and D. C. Bailey, “Limits on particles of small electric charge,” *Phys. Rev. D* **43** (1991) 2314–2321.
- [15] N. Vinyoles and H. Vogel, “Minicharged Particles from the Sun: A Cutting-Edge Bound,” *JCAP* **03** (2016) 002 [[arXiv:1511.01122](#)].
- [16] S. Davidson and M. E. Peskin, “Astrophysical bounds on millicharged particles in models with a paraphoton,” *Phys. Rev. D* **49** (1994) 2114–2117 [[hep-ph/9310288](#)].
- [17] H. Vogel and J. Redondo, “Dark Radiation constraints on minicharged particles in models with a hidden photon,” *JCAP* **02** (2014) 029 [[arXiv:1311.2600](#)].
- [18] S. Davidson, S. Hannestad, and G. Raffelt, “Updated bounds on millicharged particles,” *JHEP* **05** (2000) 003 [[hep-ph/0001179](#)].
- [19] J. H. Chang, R. Essig, and S. D. McDermott, “Supernova 1987A Constraints on Sub-GeV Dark Sectors, Millicharged Particles, the QCD Axion, and an Axion-like Particle,” *JHEP* **09** (2018) 051 [[arXiv:1803.00993](#)].
- [20] A. A. Prinz *et al.*, “Search for millicharged particles at SLAC,” *Phys. Rev. Lett.* **81** (1998) 1175–1178 [[hep-ex/9804008](#)].
- [21] E. Golowich and R. W. Robinett, “Limits on Millicharged Matter From Beam Dump Experiments,” *Phys. Rev. D* **35** (1987) 391.
- [22] D. E. Soper, M. Spannowsky, C. J. Wallace, and T. M. P. Tait, “Scattering of Dark Particles with Light Mediators,” *Phys. Rev. D* **90** (2014) 115005 [[arXiv:1407.2623](#)].
- [23] A. Berlin, N. Blinov, G. Krnjaic, P. Schuster, and N. Toro, “Dark Matter, Millicharges, Axion and Scalar Particles, Gauge Bosons, and Other New Physics with LDMX,” *Phys. Rev. D* **99** (2019) 075001 [[arXiv:1807.01730](#)].
- [24] S. N. Gninenko, D. V. Kirpichnikov, and N. V. Krasnikov, “Probing millicharged particles with NA64 experiment at CERN,” *Phys. Rev. D* **100** (2019) 035003 [[arXiv:1810.06856](#)].
- [25] X. Chu, J. Pradler, and L. Semmelrock, “Light dark states with electromagnetic form factors,” *Phys. Rev. D* **99** (2019) 015040 [[arXiv:1811.04095](#)].
- [26] L. A. Anchordoqui *et al.*, “The Forward Physics Facility: Sites, experiments, and physics potential,” *Phys. Rept.* **968** (2022) 1–50 [[arXiv:2109.10905](#)].
- [27] G. Magill, R. Plestid, M. Pospelov, and Y.-D. Tsai, “Millicharged particles in neutrino experiments,” *Phys. Rev. Lett.* **122** (2019) 071801 [[arXiv:1806.03310](#)].
- [28] R. Harnik, Z. Liu, and O. Palamara, “Millicharged Particles in Liquid Argon Neutrino Experiments,” *JHEP* **07** (2019) 170 [[arXiv:1902.03246](#)].
- [29] **ArgoNeuT** Collaboration, “Improved Limits on Millicharged Particles Using the ArgoNeuT Experiment at Fermilab,” *Phys. Rev. Lett.* **124** (2020) 131801 [[arXiv:1911.07996](#)].
- [30] **CMS** Collaboration, “Search for Fractionally Charged Particles in  $pp$  Collisions at  $\sqrt{s} = 7$  TeV,” *Phys. Rev. D* **87** (2013) 092008 [[arXiv:1210.2311](#)].
- [31] A. Haas, C. S. Hill, E. Izaguirre, and I. Yavin, “Looking for milli-charged particles with a new experiment at the LHC,” *Phys. Lett. B* **746** (2015) 117–120 [[arXiv:1410.6816](#)].
- [32] A. Ball *et al.*, “Search for millicharged particles in proton-proton collisions at  $\sqrt{s} = 13$  TeV,” *Phys. Rev. D* **102** (2020) 032002 [[arXiv:2005.06518](#)].
- [33] A. Ball *et al.*, “A Letter of Intent to Install a milli-charged Particle Detector at LHC P5.” [[arXiv:1607.04669](#)].
- [34] Z. Liu and Y. Zhang, “Probing millicharge at BESIII via monophoton searches,” *Phys. Rev. D* **99** (2019) 015004 [[arXiv:1808.00983](#)].
- [35] K. J. Kelly and Y.-D. Tsai, “Proton fixed-target scintillation experiment to search for millicharged dark matter,” *Phys. Rev. D* **100** (2019) 015043 [[arXiv:1812.03998](#)].
- [36] Z. Liu, Y.-H. Xu, and Y. Zhang, “Probing dark matter particles at CEPC,” *JHEP* **06** (2019) 009 [[arXiv:1903.12114](#)].
- [37] S. Foroughi-Abari, F. Kling, and Y.-D. Tsai, “Looking forward to millicharged dark sectors at the LHC,” *Phys. Rev. D* **104** (2021) 035014 [[arXiv:2010.07941](#)].
- [38] J. Liang, Z. Liu, Y. Ma, and Y. Zhang, “Millicharged particles at electron colliders,” *Phys. Rev. D* **102** (2020) 015002 [[arXiv:1909.06847](#)].
- [39] G. Afek, *et al.*, “Limits on the abundance of millicharged particles bound to matter,” *Phys. Rev. D* **104** (2021) 012004 [[arXiv:2012.08169](#)].
- [40] J. H. Kim, I. S. Hwang, and J. H. Yoo, “Search for sub-millicharged particles at J-PARC,” *JHEP* **05** (2021) 031 [[arXiv:2102.11493](#)].
- [41] D. Gorbunov, I. Krasnov, Y. Kudenko, and S. Suvorov, “Double-hit signature of millicharged particles in 3D segmented neutrino detector,” *Phys. Lett. B* **822** (2021) 136641 [[arXiv:2103.11814](#)].
- [42] D. Carney, H. Häffner, D. C. Moore, and J. M. Taylor, “Trapped Electrons and Ions as Particle Detectors,” *Phys. Rev. Lett.* **127** (2021) 061804 [[arXiv:2104.05737](#)].
- [43] D. Budker, *et al.*, “Millicharged Dark Matter Detection with Ion Traps,” *PRX Quantum* **3** (2022) 010330 [[arXiv:2108.05283](#)].
- [44] D. Gorbunov, D. Kalashnikov, P. Pakhlov, and T. Uglov, “On direct observation of millicharged particles at  $c\tau$  factories and other  $e^+e^-$ -colliders.” [[arXiv:2208.03377](#)].

- [45] F. Kling, J.-L. Kuo, S. Trojanowski, and Y.-D. Tsai, “FLArE up dark sectors with EM form factors at the LHC Forward Physics Facility,” [arXiv:2205.09137](#).
- [46] D. Gorbunov and D. Kalashnikov, “Probing light exotics from a hidden sector at  $c\text{-}\tau$  factories with polarized electron beams,” [arXiv:2211.06270](#).
- [47] D. E. Brahm and L. J. Hall, “U(1)-prime DARK MATTER,” *Phys. Rev. D* **41** (1990) 1067.
- [48] J. L. Feng, M. Kaplinghat, H. Tu, and H.-B. Yu, “Hidden Charged Dark Matter,” *JCAP* **07** (2009) 004 [[arXiv:0905.3039](#)].
- [49] J. M. Cline, Z. Liu, and W. Xue, “Millicharged Atomic Dark Matter,” *Phys. Rev. D* **85** (2012) 101302 [[arXiv:1201.4858](#)].
- [50] R. Barkana, N. J. Outmezguine, D. Redigolo, and T. Volansky, “Strong constraints on light dark matter interpretation of the EDGES signal,” *Phys. Rev. D* **98** (2018) 103005 [[arXiv:1803.03091](#)].
- [51] J. B. Muñoz and A. Loeb, “A small amount of mini-charged dark matter could cool the baryons in the early Universe,” *Nature* **557** (2018) 684 [[arXiv:1802.10094](#)].
- [52] A. Berlin, D. Hooper, G. Krnjaic, and S. D. McDermott, “Severely Constraining Dark Matter Interpretations of the 21-cm Anomaly,” *Phys. Rev. Lett.* **121** (2018) 011102 [[arXiv:1803.02804](#)].
- [53] R. Barkana, “Possible interaction between baryons and dark-matter particles revealed by the first stars,” *Nature* **555** (2018) 71–74 [[arXiv:1803.06698](#)].
- [54] K. K. Boddy, *et al.*, “Critical assessment of CMB limits on dark matter-baryon scattering: New treatment of the relative bulk velocity,” *Phys. Rev. D* **98** (2018) 123506 [[arXiv:1808.00001](#)].
- [55] A. Fialkov, R. Barkana, and A. Cohen, “Constraining Baryon–Dark Matter Scattering with the Cosmic Dawn 21-cm Signal,” *Phys. Rev. Lett.* **121** (2018) 011101 [[arXiv:1802.10577](#)].
- [56] E. D. Kovetz, *et al.*, “Tighter limits on dark matter explanations of the anomalous EDGES 21 cm signal,” *Phys. Rev. D* **98** (2018) 103529 [[arXiv:1807.11482](#)].
- [57] T. R. Slatyer and C.-L. Wu, “Early-Universe constraints on dark matter-baryon scattering and their implications for a global 21 cm signal,” *Phys. Rev. D* **98** (2018) 023013 [[arXiv:1803.09734](#)].
- [58] H. Liu, N. J. Outmezguine, D. Redigolo, and T. Volansky, “Reviving Millicharged Dark Matter for 21-cm Cosmology,” *Phys. Rev. D* **100** (2019) 123011 [[arXiv:1908.06986](#)].
- [59] C. Creque-Sarbinowski, L. Ji, E. D. Kovetz, and M. Kamionkowski, “Direct millicharged dark matter cannot explain the EDGES signal,” *Phys. Rev. D* **100** (2019) 023528 [[arXiv:1903.09154](#)].
- [60] A. Aboubrahim, P. Nath, and Z.-Y. Wang, “A cosmologically consistent millicharged dark matter solution to the EDGES anomaly of possible string theory origin,” *JHEP* **12** (2021) 148 [[arXiv:2108.05819](#)].
- [61] Q. Li and Z. Liu, “Two-component millicharged dark matter and the EDGES 21 cm signal,” *Chin. Phys. C* **46** (2022) [[arXiv:2110.14996](#)].
- [62] R. Plestid, *et al.*, “New Constraints on Millicharged Particles from Cosmic-ray Production,” *Phys. Rev. D* **102** (2020) 115032 [[arXiv:2002.11732](#)].
- [63] M. Kachelriess and J. Tjemsland, “Meson production in air showers and the search for light exotic particles,” *Astropart. Phys.* **132** (2021) 102622 [[arXiv:2104.06811](#)].
- [64] C. A. Argüelles Delgado, K. J. Kelly, and V. Muñoz Alborno, “Millicharged particles from the heavens: single- and multiple-scattering signatures,” *JHEP* **11** (2021) 099 [[arXiv:2104.13924](#)].
- [65] J. Alvey, M. Campos, M. Fairbairn, and T. You, “Detecting Light Dark Matter via Inelastic Cosmic Ray Collisions,” *Phys. Rev. Lett.* **123** (2019) 261802 [[arXiv:1905.05776](#)].
- [66] E. Fermi, “On the Theory of the impact between atoms and electrically charged particles,” *Z. Phys.* **29** (1924) 315–327.
- [67] E. J. Williams, “Nature of the high-energy particles of penetrating radiation and status of ionization and radiation formulae,” *Phys. Rev.* **45** (1934) 729–730.
- [68] C. F. von Weizsacker, “Radiation emitted in collisions of very fast electrons,” *Z. Phys.* **88** (1934) 612–625.
- [69] J. Blümlein and J. Brunner, “New Exclusion Limits on Dark Gauge Forces from Proton Bremsstrahlung in Beam-Dump Data,” *Phys. Lett. B* **731** (2014) 320–326 [[arXiv:1311.3870](#)].
- [70] P. deNiverville, C.-Y. Chen, M. Pospelov, and A. Ritz, “Light dark matter in neutrino beams: production modelling and scattering signatures at MiniBooNE, T2K and SHiP,” *Phys. Rev. D* **95** (2017) 035006 [[arXiv:1609.01770](#)].
- [71] Y.-D. Tsai, P. deNiverville, and M. X. Liu, “Dark Photon and Muon  $g - 2$  Inspired Inelastic Dark Matter Models at the High-Energy Intensity Frontier,” *Phys. Rev. Lett.* **126** (2021) 181801 [[arXiv:1908.07525](#)].
- [72] J. L. Feng, I. Galon, F. Kling, and S. Trojanowski, “ForwArD Search Experiment at the LHC,” *Phys. Rev. D* **97** (2018) 035001 [[arXiv:1708.09389](#)].
- [73] S. Foroughi-Abari and A. Ritz, “Dark sector production via proton bremsstrahlung,” *Phys. Rev. D* **105** (2022) 095045 [[arXiv:2108.05900](#)].
- [74] M. Du, R. Fang, Z. Liu, and V. Q. Tran, “Enhanced long-lived dark photon signals at lifetime frontier detectors,” *Phys. Rev. D* **105** (2022) 055012 [[arXiv:2111.15503](#)].
- [75] P. Gondolo, G. Ingelman, and M. Thunman, “Charm production and high-energy atmospheric muon and neutrino fluxes,” *Astropart. Phys.* **5** (1996) 309–332 [[hep-ph/9505417](#)].
- [76] C. Giunti and C. W. Kim, *Fundamentals of Neutrino Physics and Astrophysics*. 2007.
- [77] P. Lipari, “The Geometry of atmospheric neutrino production,” *Astropart. Phys.* **14** (2000) 153–170 [[hep-ph/0002282](#)].
- [78] T. Pierog, I. Karpenko, J. M. Katzy, E. Yatsenko, and K. Werner, “EPOS LHC: Test of collective hadronization with data measured at the CERN Large Hadron Collider,” *Phys. Rev. C* **92** (2015) 034906 [[arXiv:1306.0121](#)].
- [79] R. U. C. Baus, T. Pierog, “Cosmic ray Monte Carlo (CRMC).” <https://web.ikp.kit.edu/rulrich/crmc.html>.
- [80] J. Picone, A. Hedin, D. P. Drob, and A. Aikin, “NRLMSISE-00 empirical model of the atmosphere: Statistical comparisons and scientific issues,” *Journal of Geophysical Research: Space Physics* **107** (2002) SIA–15.

- [81] **Particle Data Group** Collaboration, “Review of Particle Physics,” *Phys. Rev. D* **98** (2018) 030001.
- [82] J. Liang, Z. Liu, and L. Yang, “Probing sub-GeV leptophilic dark matter at Belle II and NA64,” *JHEP* **05** (2022) 184 [[arXiv:2111.15533](#)].
- [83] K. J. Kim and Y.-S. Tsai, “IMPROVED WEIZSACKER-WILLIAMS METHOD AND ITS APPLICATION TO LEPTON AND W BOSON PAIR PRODUCTION,” *Phys. Rev. D* **8** (1973) 3109.
- [84] Y.-S. Tsai, “Pair Production and Bremsstrahlung of Charged Leptons,” *Rev. Mod. Phys.* **46** (1974) 815. [Erratum: *Rev. Mod. Phys.* 49, 421–423 (1977)].
- [85] A. Faessler, M. I. Krivoruchenko, and B. V. Martemyanov, “Once more on electromagnetic form factors of nucleons in extended vector meson dominance model,” *Phys. Rev. C* **82** (2010) 038201 [[arXiv:0910.5589](#)].
- [86] P. C. Tiemeijer and J. A. Tjon, “Electromagnetic form-factors for an off-shell nucleon in a vector meson dominance model,” *Phys. Rev. C* **42** (1990) 599–609.
- [87] T. K. Gaisser, R. Engel, and E. Resconi, *Cosmic Rays and Particle Physics: 2nd Edition*. Cambridge University Press, 2016.
- [88] J. H. Koehne, *et al.*, “PROPOSAL: A tool for propagation of charged leptons,” *Comput. Phys. Commun.* **184** (2013) 2070–2090.
- [89] V. A. Ilyin, V. V. Korenkov, and D. Perret-Gallix, eds., “The Super-Kamiokande detector,” *Nucl. Instrum. Meth. A* **501** (2003) 418–462.
- [90] **Super-Kamiokande** Collaboration, “Supernova Relic Neutrino Search at Super-Kamiokande,” *Phys. Rev. D* **85** (2012) 052007 [[arXiv:1111.5031](#)].
- [91] G. Marocco and S. Sarkar, “Blast from the past: Constraints on the dark sector from the BEBC WA66 beam dump experiment,” *SciPost Phys.* **10** (2021) 043 [[arXiv:2011.08153](#)].
- [92] N. Arefyeva, S. Gninenko, D. Gorbunov, and D. Kirpichnikov, “Passage of millicharged particles in the electron beam-dump: Refining constraints from SLACmQ and estimating sensitivity of NA64e,” *Phys. Rev. D* **106** (2022) 035029 [[arXiv:2204.03984](#)].
- [93] X. Chu, J.-L. Kuo, and J. Pradler, “Dark sector-photon interactions in proton-beam experiments,” *Phys. Rev. D* **101** (2020) 075035 [[arXiv:2001.06042](#)].
- [94] R. H. Dalitz, “On an alternative decay process for the neutral pi-meson, Letters to the Editor,” *Proc. Phys. Soc. A* **64** (1951) 667–669.
- [95] **Particle Data Group** Collaboration, “Review of Particle Physics,” *PTEP* **2020** (2020) 083C01.
- [96] S. Berman and D. Geffen, “The Electromagnetic Structure and Alternative Decay Modes of the pi0,” *Nuovo Cim.* **18** (1960) 1192.
- [97] L. G. Landsberg, “Electromagnetic Decays of Light Mesons,” *Phys. Rept.* **128** (1985) 301–376.
- [98] **NA60** Collaboration, “Precision study of the  $\eta \rightarrow \mu^+ \mu^- \gamma$  and  $\omega \rightarrow \mu^+ \mu^- \pi^0$  electromagnetic transition form-factors and of the  $\rho \rightarrow \mu^+ \mu^-$  line shape in NA60,” *Phys. Lett. B* **757** (2016) 437–444 [[arXiv:1608.07898](#)].
- [99] <https://github.com/Harvard-Neutrino/HeavenlyMCP>.